Supporting Information

Equally Efficient Interlayer Exciton Relaxation and Improved Absorption in Epitaxial and Non-epitaxial MoS_2/WS_2 Heterostructures

Yifei Yu[1§], Shi Hu[1§], Liqin Su[3§], Lujun Huang[1], Yi Liu[4], Zhenghe Jin[5], Alexander A. Purezky[6], David B. Geohegan[6], Ki Wook Kim[5], Yong Zhang[3], Linyou Cao[1,2]*

[1]Department of Materials Science and Engineering, North Carolina State University, Raleigh NC 27695; [2]Department of Physics, North Carolina State University, Raleigh NC 27695; [3]Department of Electrical and Computer Engineering, The University of North Carolina at Charlotte, Charlotte, NC 28223; [4]Analytical Instrumentation Facility, North Carolina State University, Raleigh NC 27695; [5]Department of Electrical and Computer Engineering, North Carolina State University, Raleigh NC 27695; [6] Center for Nanophase Materials Sciences, Oak Ridge National Laboratory, Oak Ridge, Tennessee 37831

[§] These authors contribute equally.

* To whom correspondence should be addressed.
Email: lcao2@ncsu.edu

This PDF file include

- Detailed structural and compositional characterizations for epitaxial MoS_2/WS_2 heterostructures.
- Fig.S1 –S8
- References S1-S8

Detailed structural and compositional characterizations for epitaxial MoS_2/WS_2 heterostructures.

Typical synthesized heterostructures consist of two concentric equilateral triangles that show obvious contrast difference under optical microscopes (Fig.S1a inset). The two triangles are usually in lateral size of from several to tens of micrometers and may be oriented in either the same or opposite directions. The shape of equilateral triangle is consistent with the hexagonal crystalline symmetry of WS_2 and MoS_2[1, 2]. It strongly suggests that the synthesized materials are single crystalline and epitaxially stacked together. Raman measurements indicate that the big triangle is monolayer MoS_2 while the small one WS_2 (Fig.S1a). The spectra collected at the region outside of the small triangle (region 1 as marked in the optical image) show the characteristic peaks A_{1g} and E^1_{2g} of MoS_2 with a frequency difference of 20.7 cm^{-1}, which well matches the frequency difference of monolayer MoS_2 reported previously[3, 4]. In contrast, the spectra collected from the small triangle (region 2 as marked) exhibit characteristic peaks of both MoS_2 and WS_2[5]. For the convenience of discussion, we refer the region 1 as MoS_2 area and the region 2 as MoS_2/WS_2 area in the following text. AFM measurements demonstrate that the heterostructure indeed consists of two monolayers stacked in the vertical direction (Fig.S1b). It shows that the first and the second layer are both in thickness of 0.7 nm, consistent with the thickness of MoS_2 and WS_2 monolayers[3]. The AFM measurement also demonstrates that the synthesized heterostructure is smooth, uniform, and continuous.

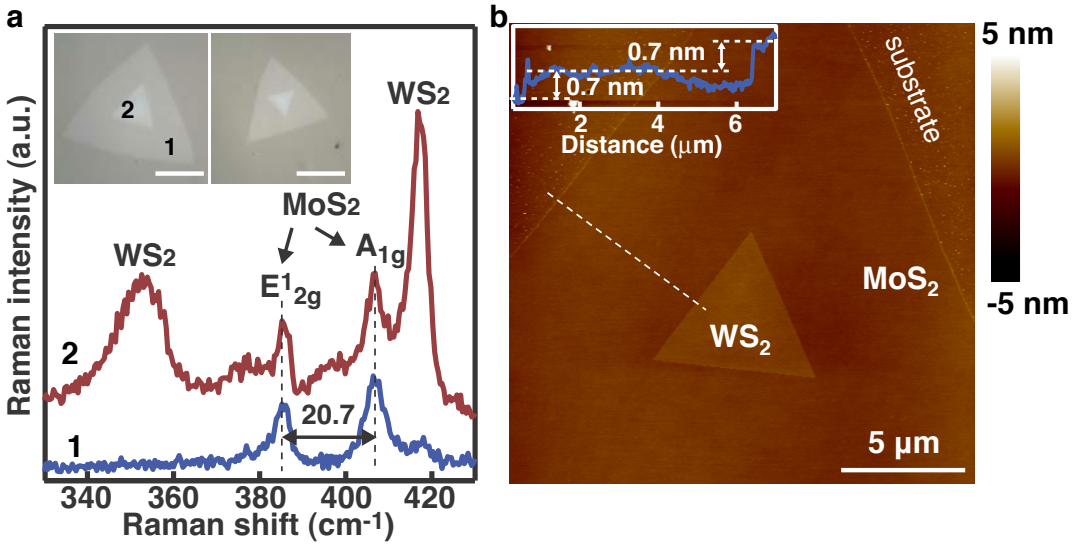

Figure S1. Synthesized epitaxial MoS_2/WS_2 monolayer heterostructures. (a) Raman spectra collected from different areas of the synthesized heterostructure. The assignment of the peaks is given in the figure. Inset, optical images of two typical MoS_2/WS_2 heterostructures with opposite relative orientations of the two triangles. The region 1 and 2 where the Raman spectra were collected from are marked. Scale bar, 10 μm. (b) AFM image of the MoS_2/WS_2 heterostructure. Inset, a typical height profile of the heterostructure as indicated by the white dashed line.

To better resolve the physical features of the heterostructure, we characterized it using an aberration-corrected scanning transmission electron microscope (STEM) that can provide atomic-scale resolution. We first transferred the heterostructure from the growth substrate

(sapphire) onto TEM grids to perform the characterization (see Methods in the text). Fig.S2a shows a typical high angle annular dark field (HAADF) image of the heterostructure. We can readily distinguish Mo and W atoms by the difference in image contrast (W atoms show higher contrast than Mo atoms). Note that sulfur atoms have very weak contrast and are difficult to be identified in the image. From the HAADF image, the lattice constants of MoS_2 and WS_2 can be found very similar as 3.16 Å, which is consistent with the results reported in literature as 3.158 Å and 3.163 Å, respectively[1, 2]. The STEM characterization confirms the epitaxial stacking of the monolayers. We performed numerous Fast Fourier transformation (FFT) in the areas of MoS_2 and MoS_2/WS_2. All ended up with identical hexagonal patterns as shown in Fig.S2a inset, indicating identical crystalline orientation in both monolayers. The STEM characterization also provides a credible way to identify the stacking sequence of the monolayers. We can find obvious offset between the atomic arrangement of the WS_2 and that of the MoS_2. The dashed orange lines, which represent the crystalline direction in the WS_2, do not pass through the MoS_2 atoms. Additionally, in the MoS_2/WS_2 area, the MoS_2 atoms (green circles) and WS_2 atoms (orange circles) form a hexagonal benzene-like structure, similar to what was found in bilayer 2H-MoS_2[3]. These indicate that the monolayers are stacked in an AB stacking mode, in which the W atoms in the WS_2 monolayer overlap with the sulfur atoms in the MoS_2 (Fig.S2b).

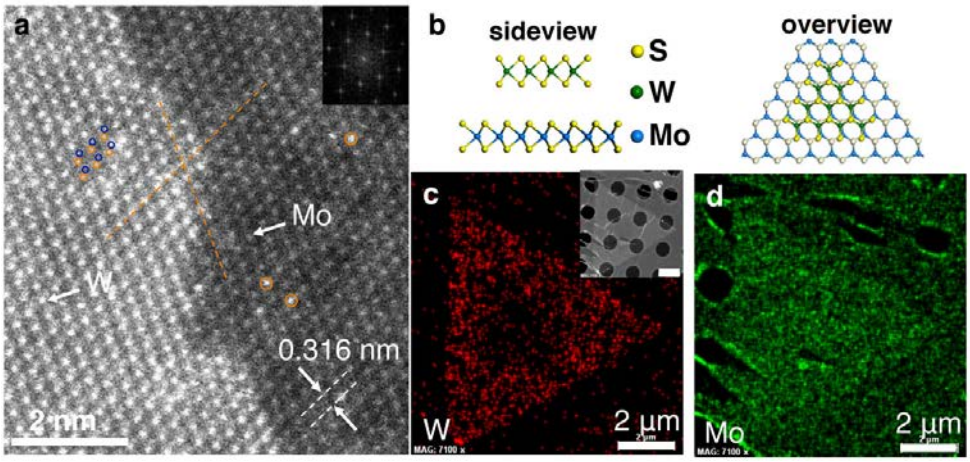

Figure S2. STEM characterizations of the synthesized MoS_2/WS_2 monolayer heterostructure. (a) High angle annular dark field image (HAADF) of the heterostructure. The W and Mo atoms that show different contrasts are denoted in the figure. The lattice constant is measured and given in the figure. The dashed orange lines indicate the crystalline directions of the WS_2 layer. The circles in orange and blue represent W and Mo atoms, respectively. Inset, a typical Fast Fourier transformation pattern of the heterostructure. (b) Sideview and overview of a structural model that shows the AB stacking of the heterostructure. The colors of the sulfur atoms in the two layers are intentionally made different in the overview for visual convenience. And EDS mapping of (c) W atoms and (d) Mo atoms of the MoS_2/WS_2 heterostructure that is shown in the inset. Scale bar of the inset: 2 μm.

Note that each of the WS_2 and MoS_2 monolayers in the heterostructure are actually alloyed with a small portion (5-10%) of the other composition. For instance, we can find W atoms with high contrast in the MoS_2 monolayer as marked by the orange circles in Fig.S2a. Energy dispersion spectrometry (EDS) elemental mapping also confirms that, while the majority of W atoms are distributed inside the MoS_2/WS_2 area, a small portion of W atoms can be found

outside (Fig.S2c). Our analysis indicates that the MoS_2 monolayer involves 5-10% WS_2 and the WS_2 monolayer 5-10% MoS_2. This alloying effect is because the growth processes of MoS_2 and WS_2 are not perfectly separated. Previous studies demonstrated that a minor alloying (5-10%) of W atoms into MoS_2 or Mo atoms into WS_2 may not cause much change in the bandstructure of the host[6]. Therefore, it is reasonable to conclude that the observed minor alloying does not affect the studies of this work. Additionally, little WS_2 can be found at the very center of the heterostructure (Fig.S2c-d). The composition can be more clearly seen in the Raman mapping of the heterostructure. The mapping measurement further indicates that there is a bilayer MoS_2 in lateral size of around 1μm at the center of the heterostructure (Fig.S3). This suggests that MoS_2 plays a key role in nucleating the heterostructure. The second layer might start with a small patch of MoS_2, which can subsequently serve as the nucleation site for the continuous growth of this layer with WS_2. Similar nucleation sites have been extensively reported in the synthesis of MoS_2 and WS_2 monolayers or fewlayers[7, 8]. Since the nucleation site (~ 1μm) only accounts a very small fraction of the heterostructure area (8-10 μm) and is at the very center, it can be readily avoided in experimental measurements and may not cause any problems for our studies either.

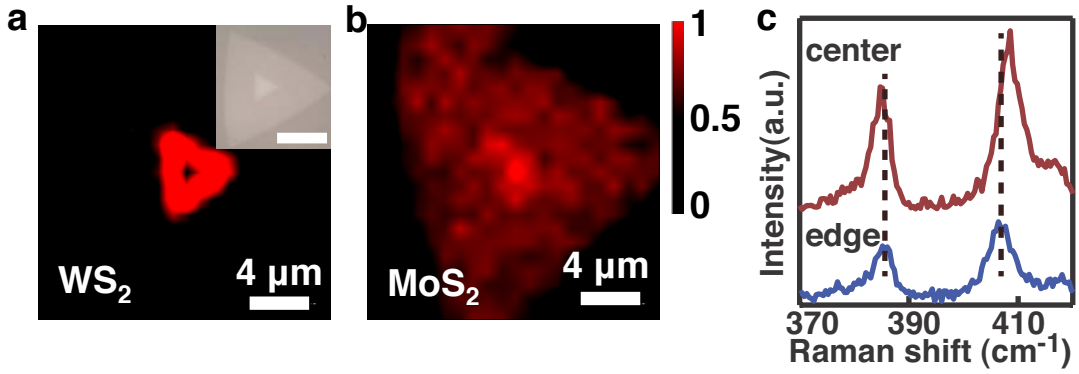

Figure S3. Raman mapping of synthesized MoS_2/WS_2 heterostructures. (a) Mapping of the Raman peaks of WS_2 for a typical heterostructure. It can be clearly seen that WS_2 is missed in a small area with a lateral size of 1 μm at the center of the heterostructure. Inset, the optical image of the heterostructure mapped. (b) Mapping of the Raman peaks of MoS_2 for the same heterostructure. The Raman intensity at the central region where WS_2 is missing shows to be particularly stronger. (c) Raman spectra collected from the very center and the MoS_2 area (edge) of the synthesized heterostructure. These two spectra show a substantial difference in the frequency difference of the two characteristic peaks, which is 20.7 cm^{-1} at the spectrum of the edge and 23.2 cm^{-1} at the one of the center. Additionally, the Raman peaks of the center show intensities around twice as large as those of the edge. These results indicate that there is bilayer MoS2 at the center of the heterostructure.

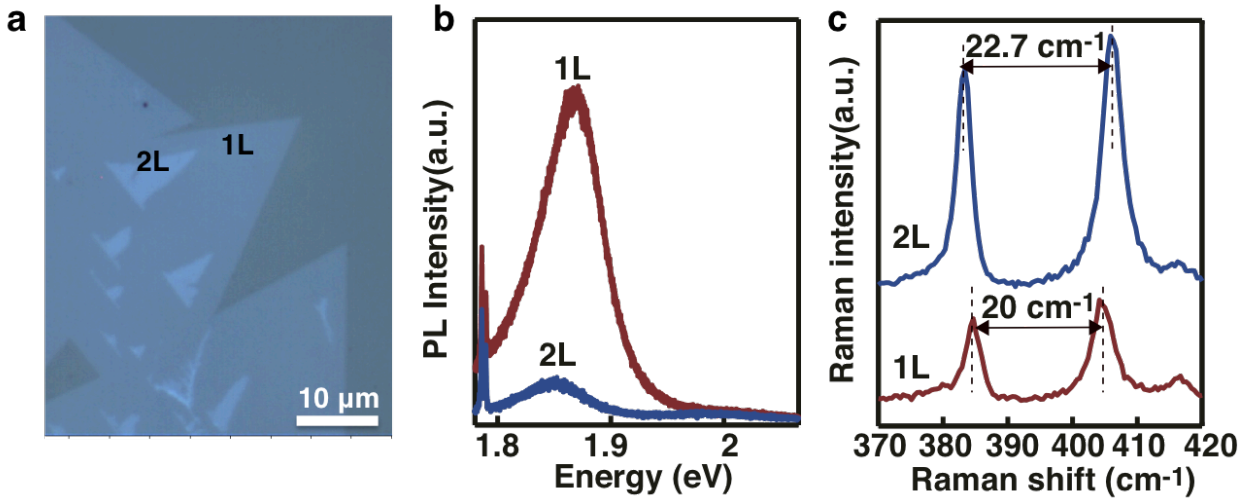

Figure S4. Characterizations of the synthesized monolayer (1L) and bilayer (2L) MoS_2. (a) optical images, (b) spectral photoluminescence (PL), and (c) Raman spectra of 1L and 2L MoS_2. The MoS_2 was made using the process described in the Methods of the main text. There are always some monolayer MoS_2 with an extra layer of flake on the top. The nice alignment of the edges of the extra layer and those of the underneath monolayer suggests the extra layer is epitaxially grown on the monolayer MoS_2. The PL of the bilayer MoS_2 shows much weaker intensity and a redshift in the peak position compared to the PL of the monolayer MoS_2. The frequency differences of the two characteristic peaks at the monolayer and bilayer MoS_2 are 20 cm^{-1} and 22. 8 cm^{-1}, respectively.

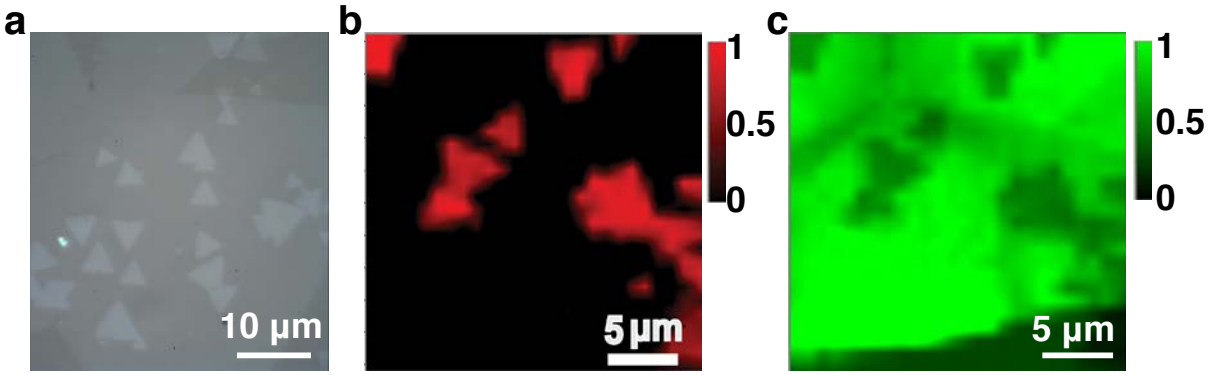

Figure S5. Characterizations of non-epitaxial MoS_2/WS_2 heterostructures made by manually stacking. (a) Optical image of a typical manually stacked MoS_2/WS_2 heterostructures. The small triangles are monolayer MoS_2 (bright) and the big triangle with weak contrast underneath is monolayer WS_2. (b) Mapping of the Raman peaks of MoS_2 and (b) of WS_2 in part of the area given in (a).

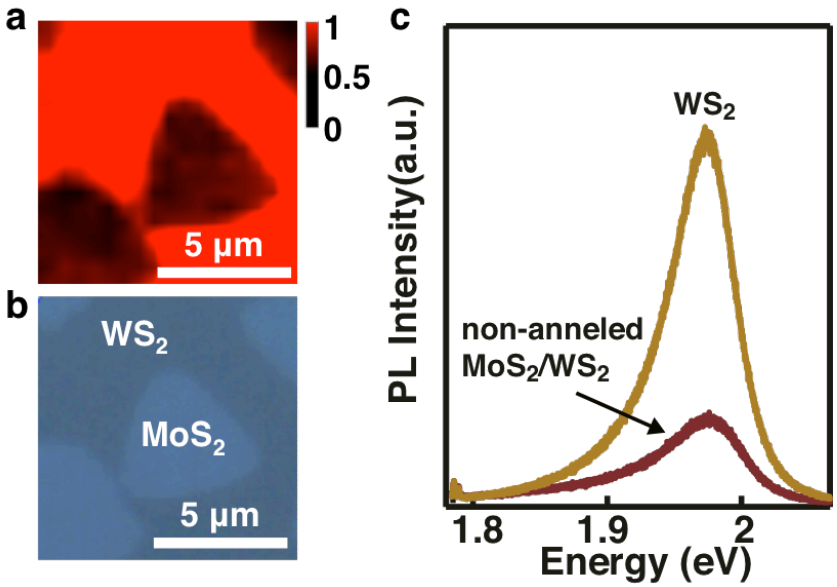

Figure S6. Characterizations of the as-prepared (non-annealed) non-epitaxial MoS_2/WS_2 heterostructures with no annealing treatment. (a) PL mapping of a typical as-prepared non-epitaxial MoS_2/WS_2 heterostructure. (b) Optical image of the heterostructure mapped in (a). (c) Spectra PL from the as-prepared non-epitaxial MoS_2/WS_2 heterostructure (red curve) and monolayer (1L) WS_2 (brown curve).

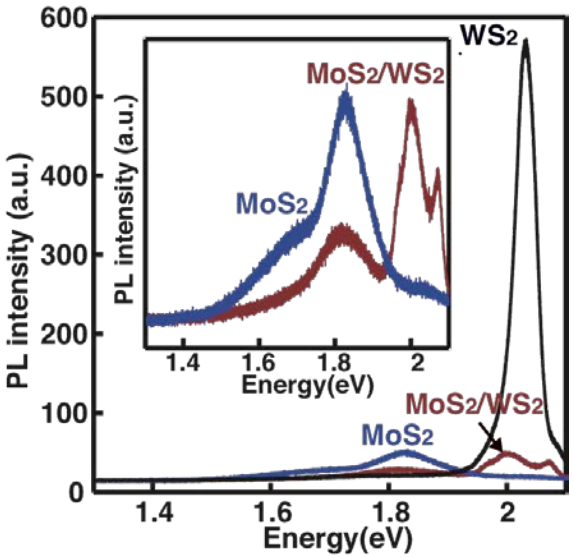

Figure S7. Spectral PL of non-epitaxial MoS_2/WS_2 heterostructures (red curve), monolayer MoS_2 (blue curve), and monolayer WS_2 (black curve) at a temperature of 10 K. The substrate used here is Si substrates with 300 nm thick thermal oxide. The inset is a zoom-in version for the results of monolayer MoS_2 and MoS_2/WS_2 heterostructures, which is to illustrate the substantial PL from the heterostructure.

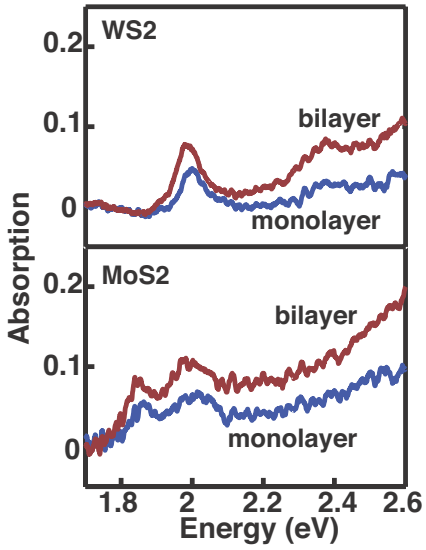

Figure S8. Absorption spectra of monolayer and bilayer WS2 (upper) and of monolayer and bilayer MoS_2 (lower).

References

S1. Schonfeld, B.; Huang, J.; Moss, S. *Acta Crystallogr. Sect. B-Struct. Sci.* **1983,** 39, 404-407.

S2. Schutte, W.; De Boer, J.; Jellinek, F. *J. Solid State Chem.* **1987,** 70, 207-209.

S3. Yu, Y. F.; Li, C.; Liu, Y., et al. *Sci. Rep.* **2013,** 3, 1866.

S4. Lee, C.; Yan, H.; Brus, L. E., et al. *ACS Nano* **2010,** 4, 2695-2700.

S5. Berkdemir, A.; Gutierrez, H. R.; Botello-Mendez, A. R., et al. *Sci. Rep.* **2013,** 3, 1755.

S6. Chen, Y. F.; Xi, J. Y.; Dumcenco, D. O., et al. *ACS Nano* **2013,** 7, 4610-4616.

S7. Najmaei, S.; Liu, Z.; Zhou, W., et al. *Nat. Mater.* **2013,** 12, 754-759.

S8. van der Zande, A. M.; Huang, P. Y.; Chenet, D. A., et al. *Nat. Mater.* **2013,** 12, 554-561.